King's Research Portal

Document Version
Peer reviewed version

[Link to publication record in King's Research Portal](#)

Journal Name

ARTICLE

Bright conjugated polymer nanoparticles containing a biodegradable shell produced at high yields and with tuneable optical properties by a scalable microfluidic device

T. F. Abelha[a], T. W. Phillips[d], J.H. Bannock[d], A. M. Nightingale[e], C. A. Dreiss[a], E. Kemal[b], L. Urbano[a], J.C. deMello[d], M. Green*[b], L. A. Dailey*[c]

This study compares the performance of a microfluidic technique and a conventional bulk method to manufacture conjugated polymer nanoparticles (CPNs) embedded within a biodegradable poly(ethylene glycol) methyl ether-block-poly(lactide-co-glycolide) (PEG_{5K}-$PLGA_{55K}$) matrix. The influence of PEG_{5K}-$PLGA_{55K}$ and conjugated polymers cyano-substituted poly(p-phenylene vinylene) (CN-PPV) and poly(9,9-dioctylfluorene-2,1,3-benzothiadiazole) (F8BT) on the physicochemical properties of the CPNs was also evaluated. Both techniques enabled CPN production with high end product yields (~70-95%). However, while the bulk technique (solvent displacement) under optimal conditions generated small nanoparticles (~70-100 nm) with similar optical properties (quantum yields ~35%), the microfluidic approach produced larger CPNs (140-260 nm) with significantly superior quantum yields (49-55%) and tailored emission spectra. CPNs containing CN-PPV showed smaller size distributions and tuneable emission spectra compared to F8BT systems prepared under the same conditions. The presence of PEG_{5K}-$PLGA_{55K}$ did not affect the size or optical properties of the CPNs and provided a neutral net electric charge as is often required for biomedical applications. The microfluidics flow-based device was successfully used for the continuous preparation of CPNs over a 24 hour period. On the basis of the results presented here, it can be concluded that the microfluidic device used in this study can be used to optimize the production of bright CPNs with tailored properties with good reproducibility.

Introduction

Conjugated polymers are materials that have semiconducting properties and strong photo/electroluminescence[1]. They have the benefit of being processable thin film materials, leading to a diverse range of technological applications[1–3]. Since the characterisation of the properties of the first generation material, polyacetylene[4,5], innovative conjugated polymer-based materials have been developed initially for optoelectronic devices (such as light-emitting diodes and photodiodes)[2,6,7] and later for highly sensitive fluorescent biosensors[8,9]. More recently CPNs have emerged as versatile materials for biomedical applications[10,11].

Cyano-substituted poly(p-phenylene vinylene) (CN-PPV) is a conjugated polymer that was first developed as a high-electron-affinity polymer for organic light-emitting diodes (OLEDs)[12]. It has a planar backbone with long alkoxy side groups[13] and strong electron withdrawing cyano (CN) groups that lead to strong intermolecular interactions[14–16]. The red or near-infrared luminescence emission[16] of CN-PPV-based materials led to their use in cell labelling[17–19], protein detection[20] and *in vivo* imaging[21]. Poly(9,9-dioctylfluorene-2,1,3-benzothiadiazole) (F8BT) is another conjugated polymer that has attracted attention for application as a diagnostic agent due to its strong photoluminescence and high quantum yields[22,23]. F8BT is a polyfluorene-based material that emits green-yellow luminescence[24]. Developed originally for OLED[24] applications, F8BT has a 2,1,3-benzothiadiazole group (BT) attached to a fluorene backbone[25]. Figure 1 shows the chemical structures and absorbance/emission spectra of both materials in tetrahydrofuran (THF).

[a.] King's College London, Institute of Pharmaceutical Science, Waterloo Campus, SE1 9NH, London, UK.
[b.] King's College London, Department of Physics, Strand Campus, WC2R 2LS, London, UK. Email: mark.a.green@kcl.ac.uk
[c.] Institut für Pharmazeutische Technologie und Biopharmazie, Martin-Luther-Universität Halle-Wittenberg, Halle, Germany. Email: lea.dailey@pharmazie.uni-halle.de
[d.] Imperial College London, Department of Chemistry, South Kensington Campus, SW7 2AZ, London, UK.
[e.] Faculty of Engineering and the Environment, University of Southampton, Southampton, UK.
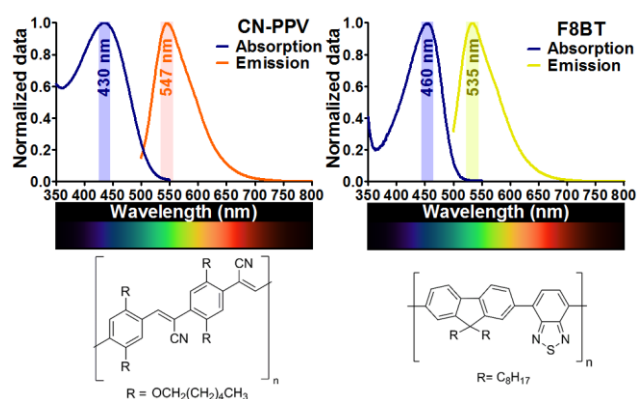
Figure 1: CN-PPV and F8BT chemical structures and their absorption and emission spectra in THF. CN-PPV has a characteristic PPV distyrylbenzene backbone with alkoxy (OC_6H_{13}) side chains and CN groups, while F8BT has a phenylene backbone with octyl (C_8H_{17}) side chains.

The material composition of CPNs influences their properties in biological fluids and cell culture media. For example, our earlier work has demonstrated that the type of surfactants used for nanoparticle assembly plays an important role in determining cellular uptake, biocompatibility and protein corona formation[26] (protein adsorption to nanoparticle surface after exposure to biological fluids[27]). Surfactants containing poly(ethylene glycol) (PEG) are commonly used for steric stabilization since they form a hydrophilic layer on the surface of the nanoparticles that prevents interactions with blood components[28]. However, we previously reported that certain types of PEGylated surfactant were prone to displacement by proteins after incubating the CPNs with serum and that the presence of unbound surfactant could cause increased haemolysis[29]. To address these issues, we propose the use of the biodegradable diblock copolymer poly(ethylene glycol) methyl ether-block-poly(lactide-co-glycolide) (PEG_{5K}-$PLGA_{55K}$) as an encapsulating agent for hydrophobic conjugated polymers. Poly(D,L-lactide-co-glycolide) (PLGA) is a biodegradable and biocompatible copolymer composed of lactic acid and glycolic acid[30]. When copolymerised with PEG, it forms a FDA-approved diblock copolymer with versatile applications[31]. PEG-PLGA self-assembles in aqueous solutions and the PLGA hydrophobic core allows the solubilisation of lipophilic compounds, while PEG imparts a stealth behaviour (prevent immunological recognition by reducing interaction with proteins[32]) for the system[31].

To enable CPNs to be used for biomedical research and future commercial applications, production methods are required that can be easily scaled from laboratory to commercial batch sizes. To be viable, any such method should exhibit excellent reproducibility with excellent yields and allow the production of nanoparticles over a range of concentrations. In this context, the present study compares a continuous flow-based procedure with a conventional bulk technique for the preparation of nanoparticles containing CN-PPV or F8BT and PEG_{5K}-$PLGA_{55K}$.

Solvent displacement, also referred as nanoprecipitation, is a conventional bulk production technique that has been widely used to manufacture PLGA-based nanoparticles[31,33]. In this method, the polymers are dissolved in a water-miscible organic solvent, which is added dropwise to water under stirring[33,34]. As a result, there is an inhomogeneous mixing of the organic and aqueous solvents due to the turbulence caused by magnetic stirring[35] and the incorporation of small volumes of polymer solution to a greater volume of water[34]. In contrast, the microfluidic system creates a well-defined reaction environment with rapid mixing of distinct volumes, thus enabling continuous production with precise control of experimental conditions[36,37,38]. Moreover, microfluidics systems are amenable to the high volume production of nanostructures[39] with the advantage of often requiring reduced amount of reagents[40] due to higher yields. Microfluidic devices based on rapid laminar flow mixing (known as hydrodynamic flow focusing) have been successfully used to prepare nanoparticles of $PEG_{3.4K}$-$PLGA_{15K}$ encapsulating docetaxel[34], of lipid-PEG/PLGA associated with quantum dots[41] and of methoxyl PEG-PLGA ($MPEG_{5K}$–$PLGA_{27K/55K/95K}$)[42]. Additionally, a droplet-based microfluidic device has been used to synthesize highly monodisperse nanoparticles of polyfluorene and poly(vinyl alcohol) with controllable diameters in the range 150 nm to 2 μm[43]. In this study, a T-junction[39] interfaced with silica capillaries was used to generate a stable and continuous reagent flow. By adjusting the infusion rates of organic and aqueous phases, CPNs of controllable size were prepared with a biodegradable shell encapsulating two different conjugated polymers.

The nanoparticle assembly is governed by the same mechanisms (i.e. nanoprecipitation) for the bulk and microfluidic methods: a solution of polymers in a water miscible organic solvent is mixed with a non-solvent of the polymers (generally water)[33,34,44,45]. The PEG-PLGA block copolymers self-assemble into nanoparticles when they experience a change from organic to aqueous solvent[45]. The dilution into a "poorer" solvent initiates a nucleation process; the nuclei grow in size by incorporating more units until becoming saturated and kinetically "locked" nanoparticles are formed[34]. Consequently, nanoparticles form instantaneously by precipitation of the polymer, after which the organic solvent can be removed by evaporation[44–46].

Despite sharing the same mechanism of nanoparticle assembly, the microfluidic and solvent displacement methods present different organic/aqueous phase mixing conditions. Here we compare the two methods by testing two conjugated polymers with distinct chemical structures. The structure of CN-PPV allows the formation of nanoparticles in the absence of an amphiphilic stabilising molecule, sharing similar self-assembling characteristics to those previously described for CN-substituted distyrylbenzenes[47] and other derivatives of PPV[48], while F8BT only forms nanoparticles in the presence of surfactants.

CPNs produced by the two techniques were evaluated with regard to their size distribution, zeta potential, emission spectra, photoluminescence (PL) quantum yields and the

reaction yield after nanoparticle production. A previous study comparing a bulk method with a hydrodynamic flow focusing device demonstrated that $PEG_{3.4K}$-$PLGA_{15K}$ nanoparticles generated by microfluidics displayed improved characteristics (smaller size/polydispersity and improved drug loading/release)[34]. Therefore, we hypothesized that CPNs produced using the microfluidic device would have a superior quality (smaller size, lower polydispersity and higher product yield) than systems produced by solvent displacement and, most importantly, we also postulated that CPNs prepared by the different techniques would have the same optical properties. Finally, we produced a large-scale preparation of CN-PPV nanoparticles using the microfluidic device to assess its suitability for high volume CPN production. To the best of our knowledge, this is the first work to evaluate the physicochemical properties of CPNs prepared by two distinct production techniques, including a large scale microfluidic production.

Experimental

1. Materials

Conjugated polymers poly(2.5-di(hexyloxy)cyanoterephthalylidene) (CN-PPV) and poly(9,9-dioctylfluorene-2,1,3-benzothiadiazole) (F8BT); poly(ethylene glycol) methyl ether-block-poly (lactide-co-glycolide) copolymer with 50:50 ratio of lactide/glycolide (PEG_{5K}-$PLGA_{55K}$); Tetrahydrofuran (THF ReagentPlus®, ≥99.0%, catalogue # 178810); sodium chloride (NaCl), Cheminert®

Plastic Fittings and Tubing (PTFE) and 5 mL glass syringe with 10.301 mm diameter (21965-U, Supelco) were supplied by Sigma-Aldrich Corporation (St. Louis, MO, USA). Synthetic fused silica capillary tubing TSP320450 and TSP100245 was supplied by (Polymicro Technologies LLC, Phoenix, Arizona, USA). HSW NORM-JECT® 20 mL 2-part disposable syringe with 20.05 mm diameter was acquired from Henke Sass Wolf GmbH (Tuttlingen, Germany). Syringe pumps Harvard Apparatus 11 plus, 11 Elite and PHD 2000 or were acquired from Harvard Apparatus (Massachusetts, U.S.A.). Flangeless Ferrule, for 1.8 mm OD Tubing, M6 or 1/4"-28 Flat Bottom, ETFE, Green (P-342X); Flangeless Ferrule, for 2.0 mm OD Tubing, M6 or 1/4"-28 Flat Bottom, ETFE, Red (P-363R); Flangeless Fitting, for 1/8" OD Tubing, 1/4"-28 Flat Bottom, Delrin/ETFE, Green/Yellow (XP-305); Adapter, Luer to 1/4"-28 Flat Bottom, ETFE (P-678) were purchased from Kinesis (Cambridgeshire, UK). Chemicals were used as received without further purification.

2. Preparation of nanoparticles

CN-PPV and F8BT nanoparticles were prepared with a ratio of 1:10 (conjugated polymer:PEG_{5K}-$PLGA_{55K}$)by two methods: a bulk method (solvent displacement) and a continuous fabrication technique (microfluidics), including a high volume microfluidic batch produced over a period of 24 hours. After production, the formulations were evaluated visually with respect to precipitation, flocculation and polymer attachment to the stirrer and flask wall. All nanoparticles were characterized without filtration or purification.

Table 1: List of conditions investigated to manufacture CN-PPV and F8BT CPNs in a continuous process.

Feed solution concentration	THF flow rate (μL/min)	H_2O flow rate (μL/min)	Flow rate ratio (THF:H_2O)	Total solids concentration in product [mg/mL]	CPN abbreviation THF:H_2O* [mg/mL]
2.4 mg/mL (10% CN-PPV: 90% PEG_{5K}-$PLGA_{55K}$)	69	111	1:1.7	1.4	**1:2[1.4]**
	53	127	1:2.4	1.0	**1:2.5[1.0]**
	53	127	1:2.4	1.0	**1:2.5[1.0] Scale up****
	31	149	1:4.8	0.5	**1:5[0.5]**
	17	163	1:9.7	0.3	**1:10[0.3]**
	12	168	1:14.5	0.2	**1:15[0.2]**
1.1 mg/mL (10% CN-PPV: 90% PEG_{5K}-$PLGA_{55K}$)	69	111	1:1.7	0.7	**1:2[0.7]**
	31	149	1:4.8	0.2	**1:5[0.2]**
0.2 mg/mL 100% CN-PPV	53	127	1:2.4	0.1	**1:2.5[0.1]**
2.4 mg/mL (10% F8BT: 90% PEG_{5K}-$PLGA_{55K}$)	69	111	1:1.7	1.4	**1:2[1.4]**
	12	168	1:14.5	0.2	**1:15[0.2]**
1.1 mg/mL (10% F8BT: 90% PEG_{5K}-$PLGA_{55K}$)	69	111	1:1.7	0.7	**1:2[0.7]**

*For the sake of clarity, the flow rate ratios have been rounded to the nearest integer or half integer in abbreviations used for the text and figures. ******One high volume batch was produced by running the microfluidics system continuously for 24 hours using the flow rate ratio and feed solution concentration listed here.

Journal Name

ARTICLE

2.1. Standard and scale up microfluidics

The microfluidic device comprised two syringe pumps connected by plastic tubing to a T-junction formed from 1 mm through-channels interfaced with silica capillaries (ESI Figure S1). Small-scale batches (i.e. standard) were prepared by injecting a fixed volume of 1 mL of THF polymer feed solution leading to formulations which varied in their final volume depending on the flow rate ratio of THF to water used (Table 1). CPNs were stirred continuously for up to 12 hours to allow complete evaporation of THF and the volume of water lost due to evaporation was replaced.

Small batch CN-PPV formulations were prepared using different flow rate ratios using the same THF feed solution concentration and a lower feed concentration at two flow rate ratios. In addition, one batch of CN-PPV nanoparticles without PEG_{5K}-$PLGA_{55K}$ was produced using a 1:2.5 (THF:H_2O) flow rate ratio. F8BT nanoparticles were prepared using a 2.4 mg/mL F8BT + PEG_{5K}-$PLGA_{55K}$ THF feed solution and two flow rate ratios (1:2 and 1:15) contrasting these with F8BT nanoparticles prepared using 1.1 mg/mL F8BT + PEG_{5K}-$PLGA_{55K}$ THF feed solution and a high THF:H_2O flow rate ratio of 1:2. Please refer to Table 1 for a summary of the conditions. At least three independent replicate batches of each formulation were produced and characterized.

A high volume microfluidic production run was carried out with the same microfluidics device connected to three dual-syringe pumps (one pump for organic phase and two for water), which were operated simultaneously to allow injection of organic/aqueous phases continuously for 24 hours (e.g. scale up). A single CN-PPV batch was produced with a flow rate ratio of 1:2.5 (THF:H_2O) using a 2.4 mg/mL polymeric feed solution (Table 1). Over the duration of the run, approximately 76 mL of THF feed solution was injected, leading to the production of approximately 183 mL of CPN solution with a final total solids concentration of 1.0 mg/mL. During the first eight hours of production, 4 mL samples were removed every two hours (in-process controls) and stirred separately, while the final product was collected in a single batch. Samples and the final product were stirred until complete evaporation of the THF had occurred. Finally, the volume of water lost due to evaporation was replaced and final product and in-process samples were characterized in triplicate.

2.2. Solvent displacement

CN-PPV and F8BT solvent displacement formulations (ESI Figure S2) were prepared with total solids concentrations of 1.4 and 0.2 mg/mL in the end product, values which were chosen to match as the microfluidic products with the highest and lowest total solids concentrations. THF (1 mL) containing either 7.2 or 0.9 mg/mL total polymer (10% w/w conjugated polymer and 90% PEG_{5K}-$PLGA_{55K}$) was added dropwise to 5 mL of water at room temperature stirred for up to 12 hours to allow complete evaporation of THF. The volume of water lost due to evaporation was replaced. One formulation containing 100% PEG_{5K}-$PLGA_{55K}$ was prepared as a control. At least three independent replicate batches of each formulation were produced and characterized.

3. Instrumentation

Product yield was defined as the measured concentration of conjugated polymer in a defined volume of end product expressed as a percentage of the theoretical concentration of conjugated polymer assuming zero loss. Duplicate samples (50-200 μL) of each CPN were dried in an oven and solubilised in 1 mL of THF prior to absorbance measurements. CN-PPV and F8BT calibration curves were prepared in THF in the concentration range of 0.8-25.0 μg/mL and absorbance assessed in a UV spectrometer (Lambda 35, Perkin Elmer Inc., USA) at 430/460 nm, respectively.

Hydrodynamic diameters were assessed by dynamic light scattering (DLS) using a Zetasizer NanoZS (Malvern Instruments Ltd, UK) at 25°C with a scattering angle of 173° and 50 μg/mL final polymer concentration. The Z-average value obtained from the intensity distribution of particles size was used to express the DLS results (all samples were monomodal). Additionally, the high volume CN-PPV batch was assessed by transmission electron microscopy (TEM) on a Tecnai 20 (FEI, EUA) at 200 kV for high resolution imaging by drop casting and drying samples on carbon film copper grids. From TEM images, the nanoparticle core size distribution was determined using ImageJ software[49]. The zeta potential at 25°C, after sample dilution in NaCl 10 mM at final polymer concentration of 20 μg/mL, was measured in a Zetasizer NanoZS (Malvern Instruments Ltd, UK).

Absorbance spectra of the CN-PPV and F8BT THF solution in the concentration range 0.8-25.0 μg/mL were acquired using a UV spectrometer (Lambda 35, Perkin Elmer Inc., USA). The PL spectrum of conjugated polymers dissolved in THF and nanoparticles diluted in water at 10.0 μg/mL CN-PPV and 0.8 μg/mL F8BT were measured in a luminescence spectrometer (LS50B, Perkin Elmer Inc., USA). Samples were analysed with the following settings: 430 nm (CN-PPV) and 470 nm (F8BT) excitation wavelength, emission slit width of 4 nm, excitation slit width of 5 nm and emission scan from 500 to 800 nm. The average PL spectrum intensity of at least three independent nanoparticle batches was calculated and the results show the normalized spectra (adjusted by the maximum PL intensity

value of each sample). The absolute PL quantum yield of CN-PPV/F8BT systems at 10.0 µg/mL of conjugated polymer was measured by exciting at 430/460 nm, respectively, in an integrating sphere (Quantaurus-QY spectrometer, Hamamatsu, Japan). GraphPad Prism (version 5.00 for Windows, GraphPad Software, San Diego California, USA) was used to perform statistical (One-way ANOVA with Tukey post hoc test) and Pearson correlation analysis. Statistical significance values were described as * $p \leq 0.05$ ** $p \leq 0.01$, *** $p \leq 0.001$.

Results and discussion

A suitable production method should generate a high yield of colloidally stable nanoparticles with a narrow size distribution. Aggregated or flocculated material should be avoided since, if present, it must be separated from the final product, thus reducing the product yield. The production of self-assembling PEG_{5K}-$PLGA_{55K}$ nanoparticles containing CN-PPV or F8BT was straightforward both by the solvent displacement and microfluidic techniques. The production process required very few steps and did not involve high energy or shear forces, such as sonication. Some formulations showed a small degree of flocculation and conjugated polymer attachment to the microfluidic device and/or to the stirrer and flask wall following solvent evaporation. Therefore, the conjugated polymer content present in defined volumes of the final product was quantified and compared with the theoretical conjugated polymer content to provide a measure for the product yield.

Product yields of CN-PPV and FBBT formulations (Figure 2) produced by traditional bulk solvent displacement were all above 50%, with mean values of ~75% and 85-90% for batches produced with the lower and higher polymer concentration in the organic phase, respectively. While CN-PPV self-assembles and formed CPNs in the absence of amphiphilic stabilising molecules (100% CN-PPV formulation), the highly hydrophobic F8BT forms nanoparticles only in the presence of surfactants, and very low batch yields were obtained previously (<30%)[26]. The incorporation of conjugated polymers within a matrix of the amphiphilic PEG-PLGA diblock copolymers was found to be a successful strategy to improve product yields of these systems.

CN-PPV nanoparticles prepared in flow showed higher product yields than bulk CPNs (>70%, with mean values typically above 90%). The product yield values for F8BT showed a much greater variation (40-98%, with mean values ranging from 45-75%). Several CN-PPV formulations were produced using different flow rate ratios and feed solution concentrations specified above, but neither of these factors appeared to significantly affect the product yield. In contrast to CN-PPV, F8BT was observed to precipitate in the device, leading to greater variability and lower mean yields than for CN-PPV.
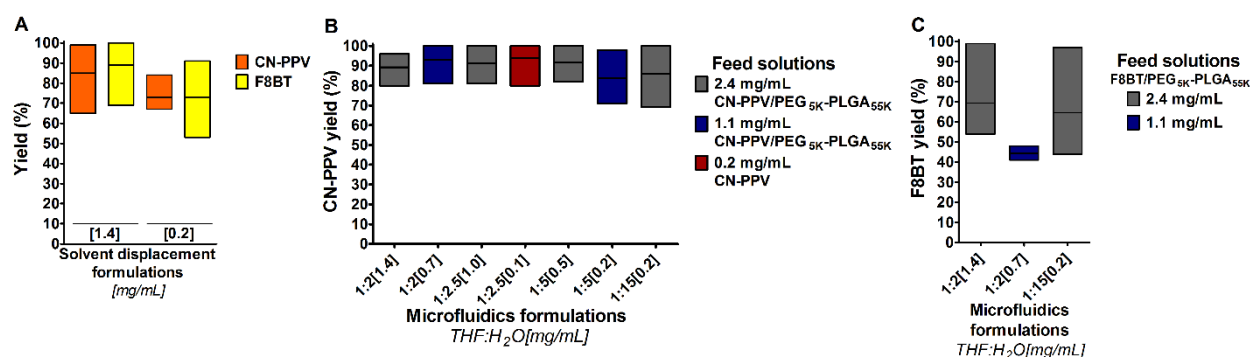

Figure 2: (**A**) Product yield (%) of CN-PPV and F8BT in formulations prepared by solvent displacement. Product yield (%) of CN-PPV (**B**) and F8BT (**C**) formulations prepared by microfluidics with different feed solution concentrations and THF:H_2O flow rate ratios. Boxes depict the maximum and minimum values with the mean values depicted through the central line crossing the box (n=3 batches).

The hydrodynamic diameters of CN-PPV and F8BT nanoparticles prepared by both microfluidic and solvent displacement techniques ranged from 75–260 nm, depending on the preparation conditions (Figure 3). Generally, the solvent displacement technique produced smaller nanoparticles (75-200 nm) than the microfluidic method (140-260 nm) and CPNs of CN-PPV were smaller than those of F8BT (Figure 3E). Reducing the polymer concentration in the organic phase of the solvent displacement method led to a decrease in particle size for both CN-PPV and F8BT nanoparticles, in agreement with previous studies[50,51].
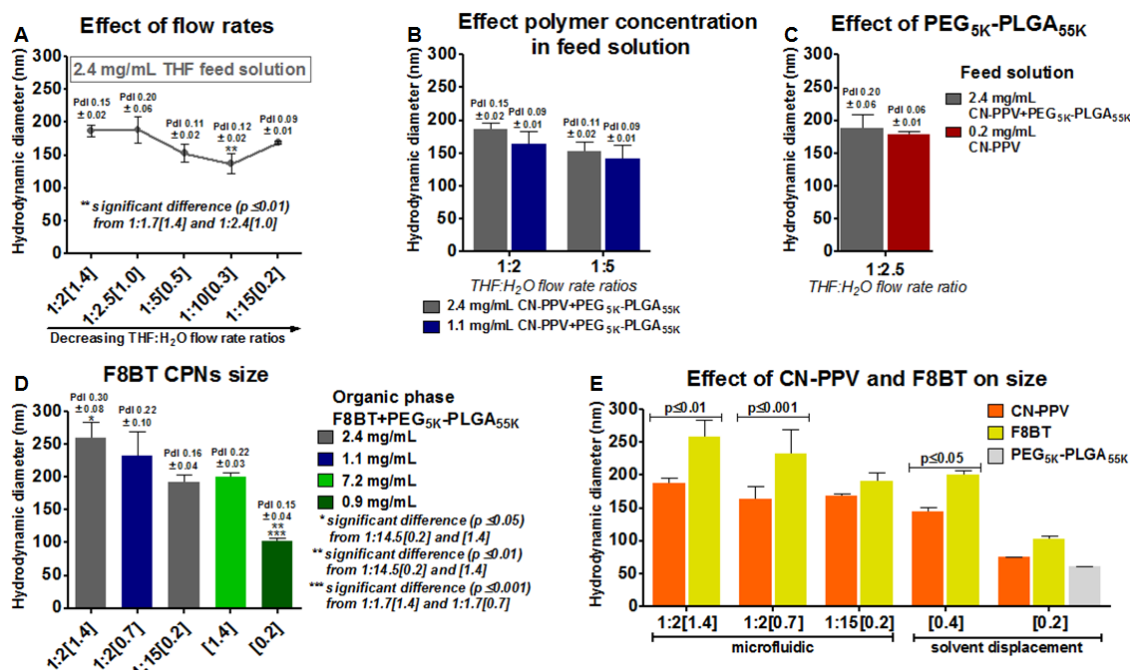
Figure 3: (**A**) Hydrodynamic diameters of CN-PPV formulations prepared by microfluidics with 2.4 mg/mL feed solution and decreasing THF:H$_2$O flow rate ratios. (**B**) Comparison of hydrodynamic diameters of CN-PPV formulations manufactured with 2.4 or 1.1 mg/mL feed solution concentrations at two THF:H$_2$O flow rate ratios. (**C**) Influence of PEG$_{5K}$-PLGA$_{55K}$ on the hydrodynamic diameter of CN-PPV nanoparticles produced with a 1:2.5 (THF:H$_2$O) flow rate ratio. (**D**) F8BT nanoparticles prepared by solvent displacement (green) and by microfluidic with two feed solutions (grey/blue) and two THF:H$_2$O flow rate ratios. (**E**) Comparison of hydrodynamic diameters of CN-PPV and F8BT microfluidics and solvent displacement CPNs, including a 100% PEG$_{5K}$-PLGA$_{55K}$ nanoparticle. Mean polydispersity values showed as PdI. Values represent the mean ± standard deviation of n=3 nanoparticle batches. * p≤0.05 ** p≤0.01, *** p≤0.001.

Changes to the microfluidic production parameters also influenced the size of CN-PPV nanoparticles. For example, maintaining a constant feed solution concentration of 2.4 mg/mL, whist decreasing the THF:H$_2$O flow rate ratio from 1:2/1:2.5 to 1:5, 1:10 and 1:15, led to a slight decrease in mean diameters from approximately 188 nm to 153 nm, 137 nm and 169 nm, respectively (Figure 3A). Although only the formulation prepared at a 1:10 (THF:H$_2$O) flow rate ratio showed a statistically significant (p≤0.01) 51 nm decrease in hydrodynamic diameter in comparison with the ones prepared under larger flow ratios (1:2 and 1:2.5). It was further noted that formulations prepared with lower THF:H$_2$O flow rate ratios generally exhibited lower polydispersity values (Figure 3A). This is in contrast with a previous study of flow-produced nanoparticles which reported that the effect of the flow rates on the size distribution of PLGA/lipid nanostructures was not significant[41]. It was also of interest to investigate whether a reduction in the microfluidics feed solution concentration from 2.4 to 1.1 mg/mL would impact the CN-PPV particle size distribution. While a reduction in the feed solution concentration led to a decrease in polydispersity index of the systems and produced a mild decrease in mean size (Figure 3B), the size reduction was not significant and the effect of reducing the flow rate ratio was much greater.

The introduction of PEG$_{5K}$-PLGA$_{55K}$ into the THF solution did not lead to a significant change in the size of CN-PPV CPNs produced by microfluidic device. Nanoparticles of 100% CN-PPV had a mean hydrodynamic diameter approximately 10 nm smaller than the equivalent formulation containing PEG$_{5K}$-PLGA$_{55K}$ (1:2.5[1.0], 188.8 ± 19.9 nm) (Figure 3C). In the case of bulk prepared materials, nanoparticles of 100% PEG$_{5K}$-PLGA$_{55K}$ presented mean hydrodynamic diameters of 60.9 ± 0.6 nm (0.20 polydispersity) and the corresponding formulation containing CN-PPV and F8BT showed a statically significant increase in size of 14 nm (p≤0.01) and of 42 nm (p≤0.001), respectively (Figure 3E). Notably, Sun et al. (2014)[17] described polyfluorene nanoparticles with size approximately three times larger than another CN-derivative of PPV prepared under the same conditions (despite using a polyfluorene with a lower molecular weight than CN-PPV). The authors rationalised the influence of the type of conjugated polymer on the size of nanoparticles on the basis of different intrinsic backbone rigidity[17]. The backbone rigidity affects the packing order of conjugated polymers and it is influenced both by the conjugated polymer main chain structure and side chains[52]. CN-PPV has a tendency to fold in unfavourable solvents[48], sharing similar self-assembling[47] characteristics to β-CN-distyrylbenzenes, due to the strong inter-chain interactions

promoted by the electron withdrawing CN groups[15,53] and π–π stacking (noncovalent interactions between aromatic rings)[47] (see Figure 1 for chemical structures). Consequently, the reduced ability of F8BT to fold during nanoparticle assembly is expected to result in a lower product yield and a larger hydrodynamic diameter compared with CN-PPV (Figure 2 and 3E, respectively). Similar to CN-PPV, a reduction in the THF:H$_2$O flow rate ratio significantly decreased the F8BT particle size and polydispersity index (p≤0.05; Figure 3D). A reduction in the feed solution concentration from 2.4 to 1.1 mg/mL also resulted in a slight, but not significant change in the mean size of F8BT CPNs.
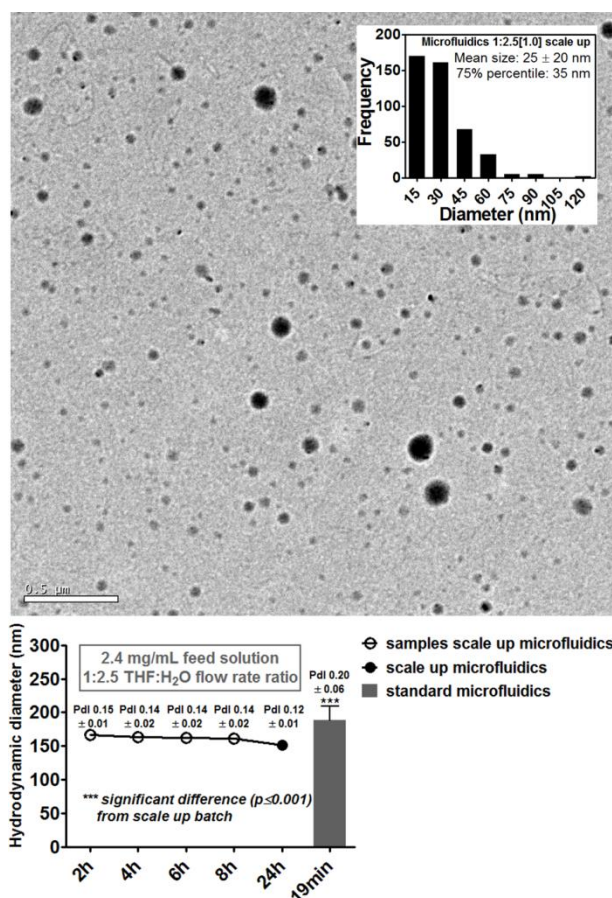

Figure 4: TEM image (scale bar 500 nm) with histogram of core size distribution of the 24-hour batch. Hydrodynamic diameters of the 24-hour batch, in-process controls and the equivalent small-scale (standard) batch of CN-PPV nanoparticles.

To assess whether increasing the volume of material produced by the microfluidic reactor had an effect on the nanoparticle size characteristics, a batch of CN-PPV nanoparticles was produced over a continuous period of 24 h (Figure 4). A 1:2.5 THF:H$_2$O flow rate ratio and 2.4 mg/mL feed solution concentration were chosen assuming close to unity yield as they would yield approximately 183 mL of CPN solution over the 24 hour duration of the collection with a high final polymer concentration (1 mg/mL). Interestingly, the

hydrodynamic diameter of the 24-hour batch (end product: 152 ± 3 nm) was significantly smaller than that of the standard batch (end product: 189 ± 20 nm; p≤0.001). The 37 nm reduction in nanoparticle diameter might be explained by the increased THF concentration present in the scale up batch over longer periods of time. More THF was continuously added over 24 hours, whereas in the standard setting a total of 1 mL of THF was injected during 19 minutes leading to a decreased THF concentration after production due to solvent evaporation. This hypothesis is supported by the slightly larger (~10 nm) hydrodynamic diameters (Figure 4) of the in-process controls which were exposed to THF for shorter periods of time compared with the end product.

TEM images of the 24-hour batch provided additional information about the size distribution and features of the CPNs produced by microfluidics (Figure 4). Due to differences in the chemical structure, it was possible to distinguish the PEG-PLGA component (i.e. the larger spheres with a low electron density) from the conjugated polymer (smaller electron-dense spheres). It appears that the CN-PPV did not mix homogenously with the PLGA core of the systems, but rather formed smaller particulates within the CPN core, as seen by the number of small, electron-dense spheres within the majority of particles in the system. Furthermore, the micrographs revealed a large population of small particles with a core size below 35 nm containing very little CN-PPV as well as larger particles with a high inclusion of CN-PPV in the core.

This polydispersity was not reflected in the DLS measurements, most likely because the population of smaller particles with low CN-PPV content would exhibit a very low scattering intensity, thereby underestimating this population in the calculation of hydrodynamic diameter. Additionally, the hydrodynamic diameter of nanoparticle systems is typically larger than the core size measurements obtained by TEM, because the hydrodynamic diameter also takes into account the solvation layer surrounding the particle[54]. This is particularly pronounced for pegylated nanoparticles, as highly hydrated PEG chains are extended in solution, a phenomenon that is not visible in TEM measurements made under dry conditions[54]. An increase of 20-30 nm for CPNs coated with PEG up to 2 kDa[54] and of approximately 40 nm[55] and 70 nm[56] for gold and polycaprolactone nanoparticles, respectively, coated with PEG 5 kDa has been reported.

The uneven distribution of conjugated polymer in the PEG-PLGA core resulting in a more polydisperse system is an undesired property from both product quality and *in vivo* performance standpoints and could be addressed in future work by exploring different PEG-PLGA chemistries, solvent systems and flow rate settings. The findings also highlight the importance of complementary analytical techniques for particle characterization.

In order to gain information on the relationship between the surface chemistry and the net electrical charge of the CPNs prepared in this study, the zeta potentials of the different nanoparticles were measured[54]. Previously, polyfluorene and poly(*p*-phenylene vinylene) derivatives incorporated into non-pegylated PLGA were reported to have a zeta potential greater

than -30.0 mV due to PLGA carboxylic acid endgroups[57], while nanoparticles of PLGA coated with PEG (PEG_{5K}-$PLGA_{28K}$) were closer to neutral (-13.8 ± 0.8 mV)[58] due to the shielding of the intrinsic negative charges of PLGA by PEG. In this study, nanoparticles consisting of 100% CN-PPV presented a highly negative zeta potential (-48.0 ± 4.9 mV) due to the surface exposure of the nucleophilic CN groups. As expected, embedding the CN-PPV and the F8BT within the core of PEG_{5K}-$PLGA_{55K}$ significantly reduced the zeta potential of the systems (Figure 5), with PEG-PLGA-coated CN-PPV nanoparticles exhibiting values ranging from -8 to-11 mV and PEG-PLGA-coated F8BT CPNs exhibiting values closer to zero (-4 to -10 mV).
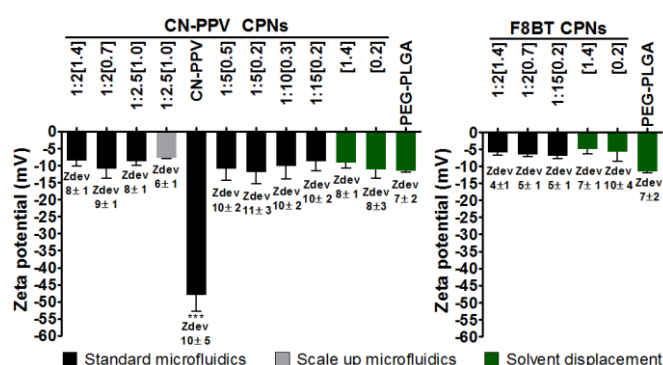

Figure 5: Zeta potential of nanoparticles containing 100% CN-PPV, 100% PEG_{5K}-$PLGA_{55K}$ and 1:10 CN-PPV/F8BT:PEG_{5K}-$PLGA_{55K}$. Values represent the mean ± standard deviation of n=3 batches. *** p≤0.001.

There is a complicated relationship between molecular conformation and the optical and electrical properties of conjugated polymers[59]. The emission spectra of organic molecules depend on environmental characteristics, such as the polarity of the medium, and on the structural features of the macromolecule (for example, its arrangement and the distribution of its chromophores)[7]. Despite the stiff aromatic backbone of the conjugated polymers, the polymer conformation can vary from a relatively opened or coil-like conformation in a good solvent to a more complex morphology in densely packed structures[17,48,60,61]. In solution, the conformation affects the extent of conjugation of a polymer and, accordingly, its optical properties[61]. For example, when polymer chains are tightly coiled due to twisting of the polymer backbone, there is a shorter average conjugation length, leading to a blue-shift of the absorption and PL spectra[53,61,62]. In packed structures, such as films and nanoparticles, adjacent chromophores are packed more closely, facilitating their interaction and leading to the formation of inter-chain species that emit at longer wavelengths than the free polymer chain[61]. The red-shifted emission is related to a low-energy absorption (π-electron density delocalized between multiple conjugated segments) and the presence of aggregates (neutral electron delocalization over multiple segments in the ground and excited states)[53,61]. Nanoparticles of conjugated polymers

typically show a red-shift emission compared to fully solvated polymers in THF, a fact that has been attributed to increased inter-chain interactions due to the compact nanoparticle conformation[17,50,51,54,63]. Moreover, a red-shift of CN-PPV emission spectra in thin films[64,65] and in poor solvent mixtures[65] has been linked to increased inter-chain interactions in previous studies. Conversely, reducing inter-chain interaction of CN-PPV derivatives by decreasing the CN content of the polymer backbone[15] or weakening CN-PPV intermolecular interactions caused by photooxidation[66], has been shown to lead to a blue shift in its luminescence spectra.
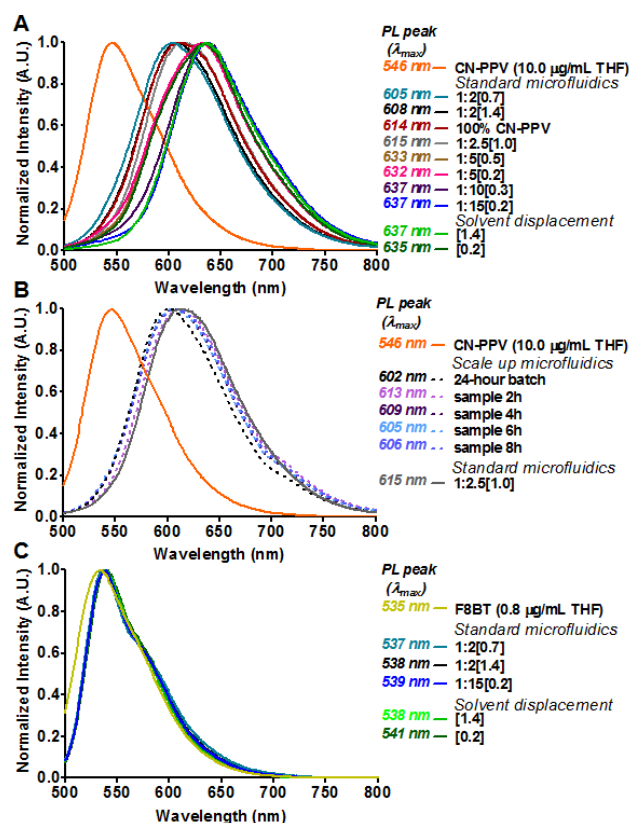

Figure 6: PL spectra of conjugated polymers in THF and of CPNs in water. (**A**) Standard microfluidics and solvent displacement CPNs containing CN-PPV. (**B**) Scale up and standard microfluidics CPNs containing CN-PPV. (**C**) Standard microfluidics and solvent displacement CPNs containing F8BT.

In this study, all CN-PPV nanoparticles showed a relatively large red-shift in the emission peak when compared to solubilized CN-PPV in THF (Figure 6). Interestingly, CN-PPV formulations prepared microfluidically at $THF:H_2O$ flow rate ratios of 1:2 and 1:2.5 exhibited smaller red shifts (59-69 nm), while nanoparticles produced at flow rate ratios of 1:5, 1:10 and 1:15 exhibited larger shifts (86-91 nm). While the flow rate ratios affected the PL spectra of CN-PPV nanoparticles, changes in the feed solution concentration did not influence the emission peaks. Moreover, PEG_{5K}-$PLGA_{55K}$ did not affect the emission maximum of CN-PPV nanoparticles: 100% CN-PPV (1:2.5[0.1]) CPNs and the equivalent system containing the same content of CN-PPV encapsulated into PEG_{5K}-$PLGA_{55K}$

(1:2.5[1.0]) presented similar emission spectra. The two solvent displacement formulations [0.2] and [1.4] presented similar emission peaks as the microfluidics formulations produced with lower flow rate ratios, showing a red-shift of 89 nm and 91 nm, respectively (Figure 6A).

A clear trend was observed between the mixing conditions of organic and water phases during production and the extent of the red-shift in emission spectra of CN-PPV. For microfluidic production, decreasing the flow rate ratio resulted in a lower relative THF concentration and higher water content during nanoparticle formation, leading to increasing red-shifts of CN-PPV emission (Figure 6A). In contrast, the mixing conditions of the traditional solvent displacement technique were heterogeneous with small amounts of organic phase being added to a greater water volume. The relatively low THF:H_2O ratio of 1:5 present in the final bulk formulation before evaporation led to a larger red-shift of about 90 nm, which is comparable to CPNs prepared in the microfluidic reactor under higher water content. Therefore, the higher content of water present during nanoparticle assembly, the bigger the red-shift in CN-PPV emission spectra. This is in accordance with previous work showing that increasing the amount of water added to THF solutions of another type of CN-PPV led to a clear red-shift in the emission spectra, which was attributed to higher inter-chain interactions and aggregation[67]. Most importantly, this demonstrates that microfluidics offers an easy means of tailoring CN-PPV emission due to the precise control of flow rates (and, accordingly, of the mixing conditions of organic and aqueous phases).

Similar effects on CN-PPV emission spectra were observed for the 24-hour batch produced by microfluidics (Figure 6B). The peak emission wavelength of the 24-hour batch was 602 nm, lower than the standard microfluidic batch (19 minutes production; 615 nm). The in-process controls exhibited emission peaks between the two values. The disparities in the peak emission wavelength can be attributed to the different mixing conditions of organic and water phases present in stirring step of the standard and scale up manufacturing process. More THF was constantly added during the 24-hour batch production, whereas 1 mL of THF was injected for the standard. Accordingly, the higher THF concentration present during the 24 h production led to smaller red-shifts. It is therefore important to note that, in spite of the rapid and steady mixing conditions present in the microfluidics coaxial flow device, the duration of solvent removal differed between the 24 h scale up and the standard batches, which had an impact on CN-PPV nanoparticle emission.

Unlike CN-PPV, the emission peaks of F8BT nanoparticles were only slightly red-shifted (2-6 nm) compared to F8BT in an organic solution (535 nm), independent of the preparation conditions (Figure 6C). Similar small red-shifts were observed for polyfluorene-derived compounds encapsulated into a PLGA matrix[57]. Moreover, the emission spectra of F8BT nanoparticles showed a pronounced long wavelength tail compared to the polymer fully solvated in THF, a fact that has been related to the production of aggregates that are red-shifted due to increased inter-chain interactions[50,51].

As the optical properties of conjugated polymers are highly sensitive to the polymer conformation and confinement[60], the PL quantum yield of selected CPNs were determined[68]. Conjugated polymers can exhibit high quantum yields depending on their chemical structure[69], including their degree of polymerization[70]. A quantum yield of 52 ± 5% has been previously reported for CN-PPV in toluene[64] and values of 42-49%[17] and ~60%[19] have been reported for nanoparticles prepared with another type of CN-PPV and the functional polymer poly(styrene-co-maleic anhydride) (PSMA). We measured similar values for CN-PPV nanoparticles prepared in our microfluidic reactor. The CPNs prepared with highest THF:H_2O flow ratio (1:2[1.4] and 1:2[0.7]) presented quantum yields of 53 ± 5% and 49 ± 2 %, respectively, while CPNs prepared using the lowest THF:H_2O flow rate (1:15[0.2]) had the lowest measured quantum yield of 40 ± 1%. The 24-hour batch and the formulation of 100% CN-PPV both had quantum yields of 48%, showing that the extended production and the inclusion of PEG_{5K}-$PLGA_{55K}$ did not interfere with the conjugated polymer emission properties. The quantum yield values obtained with the solvent displacement formulations were the lowest (36 ± 2% and 37 ± 1% for [1.4] and [0.2] CPNs, respectively), regardless of the concentration of polymers in the organic solution.

Figure 7A shows a significant (p≤0.001) negative correlation of quantum yields with and increasing PL red-shift for the CN-PPV nanoparticles, consistent with the conformational changes of the conjugated polymer backbone in confined environments[50]. It has previously been observed that a red-shift of ~20 nm led to a 8% quantum yield reduction in CN-PPV/PSMA nanoparticles[17]. Similar results were observed in this study, whereby systems with the highest red shifts (~30 nm) showed a significant (p≤0.05) quantum yield reduction of ~13%, compared to the systems with the smaller red shifts. In spite of the observed reduction in the emission efficiencies, the quantum yields of solvent displacement and microfluidic CN-PPV nanoparticles prepared in this study outperformed the values found for CPNs of another CN derivative of PPV (~27%)[18]. Finally, the hydrodynamic diameters of CN-PPV nanoparticles did not show any correlation with the quantum yield measurements (Figure 7B).
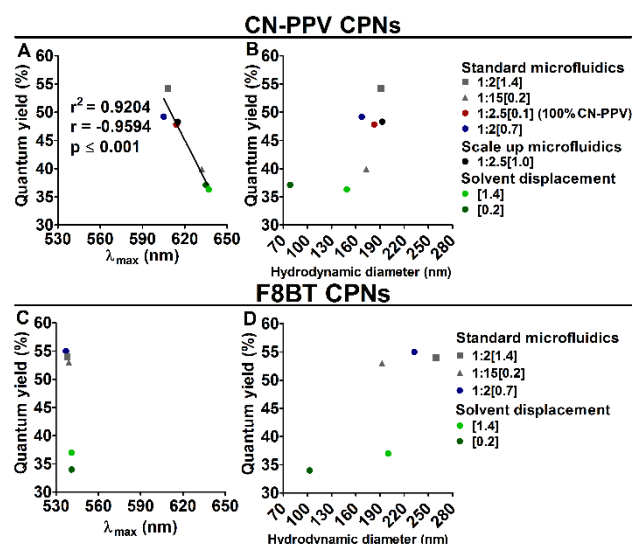
Figure 7: Correlation plots of mean quantum yield and emission peak (**A/C**) and hydrodynamic diameter (**B/D**) of CPNs prepared by microfluidic and solvent displacement techniques.

The quantum yield values of all F8BT CPNs prepared microfluidically were similar (54 ± 6% (1:1.7[1.4]), 53 ± 2% (1:14.2[0.2])) and 55 ± 6% (1:1.7[0.7])). These values are only 15% lower than those measured for the fully solvated F8BT dissolved in dichloromethane (68.6%)[23]. Moreover, F8BT nanoparticles prepared microfluidically had significantly (p<0.05) higher quantum yields than those prepared by the solvent displacement technique (37 ± 1% and 34 ± 1% for [1.4] and [0.2], respectively). A similar quantum yield of 35.8% has been observed for F8BT nanoparticles containing gadolinium produced by a bulk technique[23]. We did not observe any relationship between the size distribution or emission spectra of F8BT nanoparticles and the measured quantum yield (Figure 7C/D). Yet, it is clear that microfluidic technique produced CNPs of higher brightness than the ones prepared by solvent displacement, thus the method of nanoparticle preparation played an important role tuning F8BT nanoparticle fluorescence.

Comparing the optical properties of all the different CPNs prepared in this study, CN-PPV microfluidic systems showed more tuneable emission spectra and quantum yields than F8BT. This may be explained by the chemical structure of CN-PPV, which has strong electronegative CN groups and symmetric substitution, leading to higher interactions between polymer chains and, accordingly, an increased tendency for chain folding in solutions of unfavourable solvents (more polar)[53]. Consequently, varying the water content in the microfluidically prepared CPNs influenced the extent of CN-PPV inter-chain interactions and aggregation, resulting in nanoparticles with different optical properties. In contrast, all F8BT nanoparticles prepared microfluidically presented quantum yields above 53% and similar emission spectra, regardless of preparation conditions. Therefore, we conclude that the more rigid backbone of F8BT not only dictated the size

of the nanoparticles (as discussed previously), but also led to CPNs with similar optical properties. Conversely, the solvent displacement procedure generated CN-PPV and F8BT nanoparticles with lower quantum yields in the range of 34-37% than the ones produced microfluidically. Overall, the ratio of THF to H_2O during nanoparticle formation influenced the optical properties CN-PPV nanoparticles. The rapid and stable mixing conditions present in the microfluidics manufacturing system generated a high-yield of bright CPNs, which were colloidally stable at high total solids concentrations without the need for additional processing steps, such as dialysis or filtration. In summary, the microfluidic device used in this study provided steady and controllable production conditions that generated CPNs with readily tuneable optical properties.

Conclusions

In this work, we compared the performance of a microfluidic method and a conventional technique for producing nanoparticles of two types of conjugated polymers embedded into a biodegradable PEG_{5K}-$PLGA_{55K}$ matrix. The methods required few steps, low energy input, and no subsequent purification technique. A comparison of the two techniques revealed that nanoparticles prepared microfluidically typically had a larger particle size, a similar polydispersity and a higher product yield, but different emission spectra and higher quantum yields than CPNs prepared by flask-based solvent displacement. The size of both CN-PPV and F8BT nanoparticles could be reduced by decreasing the THF:H_2O flow rate ratio. However, this resulted in a red shift of the CN-PPV emission and a reduction in quantum yield, while the optical properties of F8BT systems were unaffected by the flow rate ratio. Interestingly, the quantum yield values of CPNs produced microfluidically were substantially higher than those produced by flask-based solvent displacement. The different chemical structure and intrinsic backbone rigidity of the two conjugated polymers appears to play an important role in determining the physicochemical properties of CPNs produced under the same conditions. The PEG_{5K}-$PLGA_{55K}$ used in this study did not influence the nanoparticle size and optical properties and provided a neutral net electrical charge to the nanoparticle surface, which may be useful for biomedical applications. Overall, the production of CPNs microfluidically promises a feasible means of producing large batch sizes, with the advantage of making it possible to tailor physicochemical and optical properties to desired specifications.

Acknowledgements

Notes and references

1   J. W. Blatchford, *Am. J. Phys.*, 1996, **64**, 120–135.
2   H. Burroughes, D. D. C. Bradley, A. R. Brown, R. N. Marks, K. Mackay, R. H. Friend, P. L. Burns and A. B. Holmes†, *Nature*, 1990, **347**, 539–541.
3   Q. Pei, *Mater. Matters*, 2007, **2**, 26–30.
4   C. K. Chiang, J. C. B. Fincher, Y. W. Park, A. J. Heeger, H. Shirakawa, E. J. Louis, S. C. Gau and A. G. MacDiarmid, *Phys. Rev. Lett.*, 1977, **39**, 1098–1101.
5   A. J. Heeger, *Chem. Soc. Rev.*, 2010, **39**, 2354–71.
6   D. Braun, *Mater. Today*, 2002, 32–39.
7   L. Akcelrud, *Prog. Polym. Sci.*, 2003, **28**, 875–962.
8   L. Chen, D. W. McBranch, H. L. Wang, R. Helgeson, F. Wudl and D. G. Whitten, *Proc. Natl. Acad. Sci. U. S. A.*, 1999, **96**, 12287–92.
9   P. S. Heeger and A. J. Heeger, *Proc. Natl. Acad. Sci. U. S. A.*, 1999, **96**, 12219–21.
10   D. Tuncel and H. V. Demir, *Nanoscale*, 2010, **2**, 484–494.
11   L. Feng, C. Zhu, H. Yuan, L. Liu, F. Lv and S. Wang, *Chem. Soc. Rev.*, 2013, **42**, 6620–33.
12   N. C. Greenham, S. C. Moratti, D. D. C. Bradley, R. H. Friend and A. B. Holmes, *Nature*, 1993, **365**, 628–630.
13   E. Conwell, J. Perlstein and S. Shaik, *Phys. Rev. B*, 1996, **54**, R2308–R2310.
14   J.-M. Park, S. K. Park, W. S. Yoon, J. H. Kim, D. W. Kim, T. Choi and S. Y. Park, *Macromolecules*, 2016, **49**, 2985–2992.
15   Z. Peng and M. E. Galvin, *Chem. Mater.*, 1998, **10**, 1785–1788.
16   X. Zhao and X. Zhan, *Chem. Soc. Rev.*, 2011, **40**, 3728–3743.
17   K. Sun, H. Chen, L. Wang, S. Yin, H. Wang, G. Xu, D. Chen, X. Zhang, C. Wu and W. Qin, *ACS Appl. Mater. Interfaces*, 2014, **6**, 10802–10812.
18   W. Zhang, H. Sun, S. Yin, J. Chang, Y. Li, X. Guo and Z. Yuan, *J. Mater. Sci.*, 2015, **50**, 5571–5577.
19   F. Ye, C. Wu, Y. Jin, M. Wang, Y.-H. Chan, J. Yu, W. Sun, S. Hayden and D. T. Chiu, *Chem. Commun. (Camb).*, 2012, **48**, 1778–80.
20   F. Ye, P. B. Smith, C. Wu and D. T. Chiu, *Macromol. Rapid Commun.*, 2013, **34**, 785–790.
21   S. Kim, C.-K. Lim, J. Na, Y.-D. Lee, K. Kim, K. Choi, J. F. Leary and I. C. Kwon, *Chem. Commun.*, 2010, **46**, 1617–1619.
22   Z. Hashim, P. Howes and M. Green, *J. Mater. Chem.*, 2011, **21**, 1797–1803.
23   Z. Hashim, M. Green, P. H. Chung, K. Suhling, A. Protti, A. Phinikaridou, R. Botnar, R. A. Khanbeigi, M. Thanou, L. A. Dailey, N. J. Commander, C. Rowland, J. Scott and D. Jenner, *Nanoscale*, 2014, **6**, 8376–8386.
24   Y. He, S. Gong, R. Hattori and J. Kanicki, *Appl. Phys. Lett.*, 1999, **74**, 2265.
25   A. Van Vooren, J. S. Kim and J. Cornil, *ChemPhysChem*, 2008, **9**, 989–993.
26   R. A. Khanbeigi, T. F. Abelha, A. Woods, O. Rastoin, R. D. Harvey, M.-C. Jones, B. Forbes, M. A. Green, H. Collins and L. A. Dailey, *Biomacromolecules*, 2015, **16**, 733–742.
27   P. Del Pino, B. Pelaz, Q. Zhang, P. Maffre, G. U. Nienhaus, W. J. Parak, P. del Pino and P. D. U. Nienhaus, *Mater. Horizons*, 2014, **1**, 301–313.
28   B. Romberg, W. E. Hennink and G. Storm, *Pharm. Res.*, 2008, **25**, 55–71.
29   R. A. Khanbeigi, Z. Hashim, T. F. Abelha, S. Pitchford, H. Collins, M. Green and L. A. Dailey, *J. Mater. Chem. B*, 2015, **3**, 2463–2471.
30   J.-S. Choi, K. Seo and J.-W. Yoo, *J. Pharm. Investig.*, 2012, **42**, 155–163.
31   K. Zhang, X. Tang, J. Zhang, W. Lu, X. Lin, Y. Zhang, B. Tian, H. Yang and H. He, *J. Control. release*, 2014, **183**, 77–86.
32   J. Wolfram, Y. Yang, J. Shen, A. Moten, C. Chen, H. Shen, M. Ferrari and Y. Zhao, *Colloids Surf. B. Biointerfaces*, 2014.
33   S. Schubert, J. T. Delaney, Jr and U. S. Schubert, *Soft Matter*, 2011, **7**, 1581.
34   R. Karnik, F. Gu, P. Basto, C. Cannizzaro, L. Dean, W. Kyei-Manu, R. Langer and O. C. Farokhzad, *Nano Lett.*, 2008, **8**, 2906–12.
35   G. Halász, B. Gyüre, I. M. Jánosi, K. G. Szabó and T. Tél, *Am. J. Phys.*, 2007, **75**, 1092.
36   G. M. Whitesides, *Nature*, 2006, **442**, 368–73.
37   J. B. Knight, A. Vishwanath, J. P. Brody and R. H. Austin, *Phys. Rev. Lett.*, 1998, **80**, 3863–3866.
38   G. Luo, L. Du, Y. Wang, Y. Lu and J. Xu, *Particuology*, 2011, **9**, 545–558.
39   A. M. Nightingale, J. H. Bannock, S. H. Krishnadasan, F. T. F. O'Mahony, S. A. Haque, J. Sloan, C. Drury, R. McIntyre and J. C. DeMello, *J. Mater. Chem. A*, 2013, **1**, 4067.
40   E. K. Sackmann, A. L. Fulton and D. J. Beebe, *Nature*, 2014, **507**, 181–9.
41   P. M. Valencia, P. A. Basto, L. Zhang, M. Rhee, R. Langer, O. C. Farokhzad and R. Karnik, *ACS Nano*, 2010, **4**, 1671–1679.
42   X. Kang, C. Luo, Q. Wei, C. Xiong, Q. Chen, Y. Chen and Q. Ouyang, *Microfluid. Nanofluidics*, 2013, **15**, 337–345.
43   A. J. C. Kuehne and D. A. Weitz, *Chem. Commun.*, 2011, **47**, 12379–12381.
44   P. Legrand, S. Lesieur, A. Bochot, R. Gref, W. Raatjes, G. Barratt and C. Vauthier, *Int. J. Pharm.*, 2007, **344**, 33–43.
45   P. M. Valencia, O. C. Farokhzad, R. Karnik and R. Langer, *Nat. Nanotechnol.*, 2012, **7**, 623–9.
46   S. Stainmesse, A.-M. Orecchioni, E. Nakache, F. Puisieux and H. Fessi, *Colloid. Polym. Sci.*, 1995, **273**, 505–511.
47   S.-J. Yoon, J. H. Kim, J. W. Chung and S. Y. Park, *J. Mater. Chem.*, 2011, **21**, 18971.
48   B. G. Sumpter, P. Kumar, A. Mehta, M. D. Barnes, W. A. Shelton and R. J. Harrison, *J. Phys. Chem. B*, 2005, **109**, 7671–7685.
49   C. A. Schneider, W. S. Rasband and K. W. Eliceiri, *Nat. Methods*, 2012, **9**, 671–675.
50   C. Wu, C. Szymanski and J. McNeill, *Langmuir*, 2006, **22**, 2956–60.
51   C. Wu, B. Bull, C. Szymanski, K. Christensen and J. McNeill, *ACS Nano*, 2008, **2**, 2415–2423.
52   K.-Y. Wu, C.-C. Chiu, W.-T. Chuang, C.-L. Wang and C.-S. Hsu, *Polym. Chem.*, 2015, **6**, 1309–1315.
53   T.-Q. Nguyen, V. Doan and B. J. Schwartz, *J. Chem. Phys.*, 1999, **110**, 4068.
54   P. K. Kandel, L. P. Fernando, P. C. Ackroyd and K. A.

Christensen, *Nanoscale*, 2011, **3**, 1037–1045.

55   Arnida, M. M. Janát-Amsbury, A. Ray, C. M. Peterson and
      H. Ghandehari, *Eur. J. Pharm. Biopharm.*, 2011, **77**, 417–
      423.

56   A. H. Johnston, P. D. Dalton and T. A. Newman, *J.
      Nanoparticle Res.*, 2010, **12**, 1997–2001.

57   K. Li, J. Pan, S. S. Feng, A. W. Wu, K. Y. Pu, Y. Liu and B. Liu,
      Adv. Funct. Mater., 2009, **19**, 3535–3542.

58   C. W. Liu and W. J. Lin, *Int. J. Nanomedicine*, 2012, **7**, 4749–
      4767.

59   C. Szymanski, C. Wu, J. Hooper, M. A. Salazar, A. Perdomo,
      A. Dukes and J. McNeill, *J. Phys. Chem. B*, 2005, **109**, 8543–
      6.

60   J. K. Grey, D. Y. Kim, B. C. Norris, W. L. Miller and P. F.
      Barbara, *J. Phys. Chem. B*, 2006, **110**, 25568–25572.

61   B. J. Schwartz, *Annu. Rev. Phys. Chem.*, 2003, **54**, 141–172.

62   J. S. Kim, L. Lu, P. Sreearunothai, A. Seeley, K. H. Yim, A.
      Petrozza, C. E. Murphy, D. Beljonne, J. Cornil and R. H.
      Friend, *J. Am. Chem. Soc.*, 2008, **130**, 13120–13131.

63   G. Padmanaban and S. Ramakrishnan, *J. Phys. Chem. B*,
      2004, **108**, 14933–14941.

64   I. D. W. Samuel, G. Rumbles and C. J. Collison, *Phys. Rev. B*,
      1995, **52**, R11573–R11576.

65   I. D. W. Samuel, G. Rumbles, C. J. Collison, S. C. Moratti and
      A. B. Holmes, *Chem. Phys.*, 1998, **227**, 75–82.

66   Y. Kuzuoka and Y. Yamaguchi, *Synth. Met.*, 2008, **158**, 489–
      496.

67   X.-T. Sun, M. Liu and Z.-R. Xu, *Talanta*, 2014, **121**, 163–77.

68   A. T. R. Williams, S. A. Winfield and J. N. Miller, *Analyst*,
      1983, **108**, 1067–1071.

69   N. C. Greenham, I. D. W. Samuel, G. R. Hayes, R. T. Phillips,
      Y. A. R. R. Kessener, S. C. Moratti, A. B. Holmes and R. H.
      Friend, *Chem. Phys. Lett.*, 1995, **241**, 89–96.

70   M. Hanack, B. Behnisch, H. Häckl, P. Martinez-Ruiz and K.-
      H. Schweikart, *Thin Solid Films*, 2002, **417**, 26–31.